J. Micromech. Microeng. **20** (2010) 045007 (8pp) doi:10.1088/0960-1317/20/4/045007

Replication performance of Si-N-DLC-coated Si micro-molds in micro-hot-embossing

B Saha[1], E Liu[2], S B Tor[1,2], N W Khun[2], D E Hardt[3] and J H Chun[3]

[1] Singapore–MIT Alliance, Nanyang Technological University, 65 Nanyang Avenue, Singapore 637460, Singapore
[2] School of Mechanical and Aerospace Engineering, Nanyang Technological University, 50 Nanyang Avenue, Singapore 639798, Singapore
[3] Department of Mechanical Engineering, Singapore–MIT Alliance, Massachusetts Institute of Technology, 77 Massachusetts Avenue, Cambridge, MA, USA

E-mail: msbtor@ntu.edu.sg

Received 26 October 2009, in final form 29 December 2009
Published 15 March 2010
Online at stacks.iop.org/JMM/20/045007

Abstract
Micro-hot-embossing is an emerging technology with great potential to form micro- and nano-scale patterns into polymers with high throughput and low cost. Despite its rapid progress, there are still challenges when this technology is employed, as demolding stress is usually very high due to large friction and adhesive forces induced during the process. Surface forces are dominating parameters in micro- and nano-fabrication technologies because of a high surface-to-volume ratio of products. This work attempted to improve the surface properties of Si micro-molds by means of silicon- and nitrogen-doped diamond-like carbon (Si-N-DLC) coatings deposited by dc magnetron cosputtering on the molds. The bonding structure, surface roughness, surface energy, adhesive strength and tribological behavior of the coated samples were characterized with micro Raman spectroscopy, atomic force microscopy (AFM), contact angle measurement, microscratch test and ball-on-disk sliding tribological test, respectively. It was observed that the doping condition had a great effect on the performance of the coatings. The Si-N-DLC coating deposited with 5×10^{-6} m^3 min^{-1} N_2 had lowest surface roughness and energy of about 1.2 nm and 38.2×10^{-3} N m^{-1}, respectively, while the coatings deposited with 20×10^{-6} and 25×10^{-6} m^3 min^{-1} N_2 showed lowest friction coefficients. The uncoated and Si-N-DLC-coated Si micro-molds were tested in a micro-hot-embossing process for a comparative study of their replication performance and lifetime. The experimental results showed that the performance of the Si micro-molds was improved by the Si-N-DLC coatings, and well-defined micro-features with a height of about 100 μm were fabricated successfully into cyclic olefin copolymer (COC) sheets using the Si-N-DLC-coated micro-molds.

1. Introduction

Carbon exists in various forms and has been used in numerous applications. Diamond-like carbon (DLC) can contain a significant amount of sp^3 bonds and have excellent characteristics such as high hardness, good chemical inertness, low surface energy, low coefficient of friction and higher wear resistance [1, 2]. These characteristics make DLC coatings useful in many applications such as cutting and forming tools, heat exchangers, high frequency and high power electronic devices, data storage systems and anti-thrombus coatings [3, 4].

However, a high internal stress occurring in DLC coatings has been a subject of recent intensive studies, as it can cause poor adhesion of the coatings with substrates and thus limits the thickness of the coatings [5–7]. Doping DLC with some metals and non-metals can tackle the above issues [8, 9].

It was reported that Si incorporated into DLC coatings could reduce the stress of the coatings, make the friction coefficient of the coatings independent of relative humidity, improve the adhesion of the coatings to substrates and increase the thermal stability of the coatings [10–12]. Incorporation of nitrogen in DLC coatings could increase the critical load and decrease the friction coefficient and stress of coatings [13, 14].

Micro-hot-embossing is an important technology in fabrication of polymeric microstructures due to its numerous advantages such as low cost and high efficiency. A typical hot-embossing process applies a temperature above glass transition temperature (T_g) of a workpiece and a high pressure to form microstructures into the workpiece [15, 16]. Both workpiece and micro-mold are subjected to heating before stamping, and a cooling process is required before demolding. To produce well-defined products with good replication requires high pressure and temperature for better mold filling [17]. However, high friction and adhesion interlocking often make demolding difficult and reduce the lifetime of molds [18, 19]. Different types of mold materials have been studied [20], among which Si is the most popular because of its well-established fabrication process and good surface finishing [21].

This work aimed to improve the surface properties of silicon micro-molds that were used for fabrication of microfluidic devices by hot-embossing. A micro-mold has a large ratio of surface area to volume, which makes it particularly vulnerable to adhesion to molded products or adjacent structures during release [18, 19]. A major design constraint for micro-molds is their inability to withstand a prolonged sliding surface contact, by which a short functional lifetime of these devices is induced through high friction or high cohesive energy of the counterparts in contact [22]. To tackle this problem, anti-sticking silicon- and nitrogen-doped diamond-like carbon (Si-N-DLC) coatings were deposited on the Si micro-molds by dc magnetron co-sputtering, and a comparative study on the performance of the coated and uncoated molds in a micro-hot-embossing process was carried out.

2. Experimental details

2.1. Deposition of DLC coatings

The DLC coatings were deposited by using dc magnetron co-sputtering that comprised carbon (C, 99.99%) and silicon (Si, 99.99%) as target materials at a pressure of about 0.4 Pa for 60 min. Si micro-molds as substrates, before they were introduced into the deposition chamber, were first rinsed with deionized (DI) water and ethanol alternately eight times to remove dirty and oily materials, after they were ultrasonically cleaned in ethanol for 20 min at 30 °C. Prior to depositions, the Si substrates were etched inside the sputtering chamber by argon (Ar) plasma for 20 min at a pressure of about 1.2 Pa and a substrate bias of −225 V. During the DLC depositions, Ar gas was introduced into the deposition chamber at a fixed flow rate of 50×10^{-6} m^3 min^{-1}. The C and Si targets were placed under a dc power of 850 W and a RF power of 25 W, respectively, and a bias voltage of −90 V was applied to the substrates during the depositions. The uniformity of the coatings was maintained with the substrates rotated at 20 rpm during deposition. Five different coatings were produced with varying N_2 flow rate starting at 5×10^{-6} m^3 min^{-1} with an even increment of 5×10^{-6} till 25×10^{-6} m^3 min^{-1}, i.e. Si-N5-DLC, Si-N10-DLC, Si-N15-DLC, Si-N20-DLC and Si-N25-DLC.

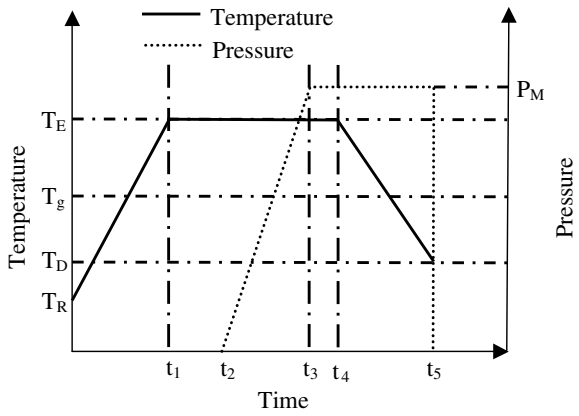

Figure 1. Schematic process profile of hot-embossing.

2.2. Hot-embossing

Micro-hot-embossing was employed to study the replication performance of the coated and uncoated Si micro-molds. Cyclic olefin copolymer (8007-COC) sheets of 1.5 mm thickness having the deflection temperature and linear expansion coefficient of 75 °C and 0.78×10^{-4} K^{-1}, respectively, were used as substrate materials in the hot-embossing process. T_g of the COC used was 78 °C, which was measured. The Si micro-molds used in the hot-embossing process were produced by a deep reactive ion-etching (DRIE) process, which was described elsewhere [9].

Hot-embossing requires a combination of three operating parameters such as temperature, pressure and time that have a great influence on the replication quality. Based on the previous experience, combined temperature and load profiles were used as presented in figure 1, which were suitable for the chosen materials and experiment setup.

In the first stage, the COC and Si micro-molds were heated to 90 °C (T_E) that was higher than T_g of COC. A constant pressure (P_M) of about 0.44 MPa at 90 °C was maintained during the second stage to form a micro-pattern into the COC substrates. The temperature was maintained at 90 °C for 4 min. In the third stage, the COC substrates and Si micro-molds were naturally cooled down to 30 °C (demolding temperature, T_D) and then the pressure was released to atmosphere. At the end, the Si micro-molds were demolded manually at 30 °C.

In this work, two types of Si micro-molds with different micro-patterns were used to study the effect of pattern on the replication performance of the molds, i.e. one had a surface area of 25.5×25.0 mm^2 with zigzag channels of 100 μm in both width and depth and 500 μm in period as shown in figure 2(*a*), and another had a square surface area of 5.94×5.94 mm^2 with parallel channels of 50, 100 and 50 μm in width, height and spacing, respectively, as shown in figure 2(*b*).

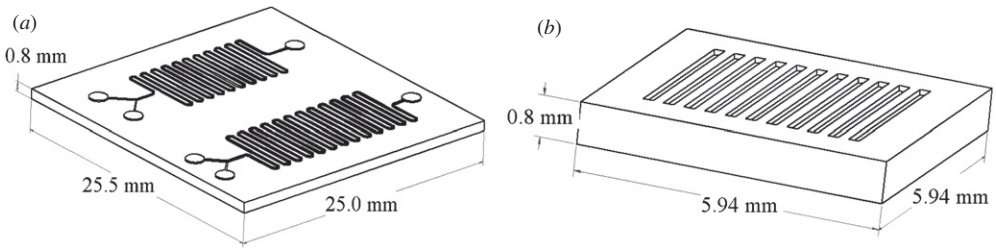

Figure 2. Schematic diagrams of micro-molds having (*a*) zigzag channels and (*b*) parallel channels.

Table 1. Total surface energies (γ_{lv}) and their polar (γ_{lv}^{p}) and dispersive (γ_{lv}^{d}) components of DI water and ethyleneglycol.

Liquid	$\gamma_{lv}^{d} \times 10^{-3}$ (N m^{-1})	$\gamma_{lv}^{p} \times 10^{-3}$ (N m^{-1})	$\gamma_{lv} \times 10^{-3}$ (N m^{-1})
DI water	21.8	51	72.8
Ethyleneglycol	29.3	19	48.3

2.3. Characterization

The bonding configurations of the Si-N-doped DLC coatings were analyzed with micro Raman spectroscopy using a He–Ne ion laser of 633 nm in wavelength. The Raman spectra were recorded from 800 to 2000 cm^{-1} and fitted with Gaussian shapes, from which peak positions, peak intensity ratio (I_D/I_G) and full width at half maximum (FWHM) were determined. The I_D/I_G ratio signifies the clustering of graphite and sp^3/sp^2 ratio of the coatings [23].

The surface roughnesses of the coated and uncoated Si micro-molds were measured by atomic force microscopy (AFM) (CSPM-4000) using a Si_3N_4 cantilever in tapping mode with a scan rate of 0.7 Hz and a scan area of 20 × 20 μm^2 inside a closed chamber at atmospheric condition.

The friction coefficient of the uncoated and DLC-coated Si micro-molds sliding against a SiC ball of 6 mm diameter was evaluated using a ball-on-disk microtribometer (CMS^{TM}) at room temperature. The ball was slid on each sample surface for 250 laps along a track of 1 mm radius at a sliding speed of 5×10^{-2} m s^{-1} and a normal load of 1 N.

The scratch test was performed on the Si-N-DLC-coated samples by a micro-scratch tester (SST-101, Shimadzu) in a progressive mode with a diamond stylus of 15 μm radius and at a scratching rate of 10 μm s^{-1}. Critical load was measured five times on each sample and scanning electron microscopy (SEM) pictures were used to study the scratch profile.

Prior to contact angle measurement, the samples were cleaned in ethanol and DI water in sequence. Contact angles were measured from DI water and ethyleneglycol drops on the sample surfaces and each sample was measured five times with an average value taken to calculate surface energy. The surface energies of the samples were calculated from the contact angles of the two liquids. The dispersive $\left(\gamma_{lv}^{d}\right)$ and polar $\left(\gamma_{lv}^{p}\right)$ components of DI water and ethyleneglycol are shown in table 1 [24].

T_g of the COC was determined by a differential scanning calorimeter (DSC) using about 10 mg COC, crimped into an aluminum pan and scanned at a heating rate of 10 °C min^{-1}.

3. Results and discussion

The Si-N-DLC coatings exhibit two broad Raman peaks at about 1350 and 1550 cm^{-1} as shown in the inserted Raman spectra in figure 3(*a*). The Raman peak at around 1550 cm^{-1} ascribed to graphitic carbon is called the G peak. A lower frequency modulus corresponding to the disordered zone becomes active at around 1350 cm^{-1} that is termed the D peak [25], which is not present in a perfect single graphite crystal. The I_D/I_G ratio, G peak position and FWHM of the coatings are presented as a function of the N_2 flow rate in figure 3(*a*). The G peak position of the Si-N-DLC coatings varies in the range of 1534 to 1578 cm^{-1}. A lower G peak position indicates a lower fraction of graphite in a coating [23]. From figure 3(*a*), it is observed that the fractions of sp^2 bonds are in the order of Si-N5-DLC < Si-N10-DLC < Si-N15-DLC < Si-N20-DLC < Si-N25-DLC. The FWHM of the G peak is observed in figure 3(*a*), which decreases with an increase in the N_2 flow rate and is inversely related to the cluster size of sp^2 zones in the coatings [23, 24]. The stress in the Si-N-DLC coatings decreases with lower sp^3 content, which allows us to form larger clusters in the coatings and decreases the degree of disorder in the coatings. A stable $FWHM_G$ is observed for the Si-N25-DLC coating because of a higher fraction of terminating bonds (C≡N) in the coatings deposited with higher N_2 flow rate. The Raman peak at around 2220 cm^{-1} is the sign of termination bonds (C≡N) as shown in figure 3(*b*). The largest peak is observed for the Si-N25-DLC coating, which indicates a higher fraction of C≡N bonds.

It is also observed that the intensity ratio (I_D/I_G) shifts to higher values with the upshift of the G peak position at higher N_2 flow rates as presented in figure 3(*a*), which also indicates decreased sp^3 bonds in the DLC coatings deposited with higher N_2 flow rates.

Figure 4 shows the surface roughnesses of the samples measured with AFM, where the average root-mean-square roughness (R_q) values are in the order of Si-N25-DLC (7.8 nm) > Si-N20-DLC (5.4 nm) > Si-N15-DLC (4.9 nm) > Si-N10-DLC (4.7 nm) > Si-N5-DLC (3.8 nm) > Si uncoated (1.1 nm). With higher N_2 flow rates, the sp^2 content is promoted in the DLC coatings, which increases the sp^2 cluster size and roughness [26] of the coatings.

The surface forces dominate the performance of the micro-molds as their surface-to-volume ratios are very high [9, 18, 19] and the functional lifetime of the Si micro-molds can be shortened by high friction, cohesive energy and wear of the mold surfaces [22]. The above problems are tackled with

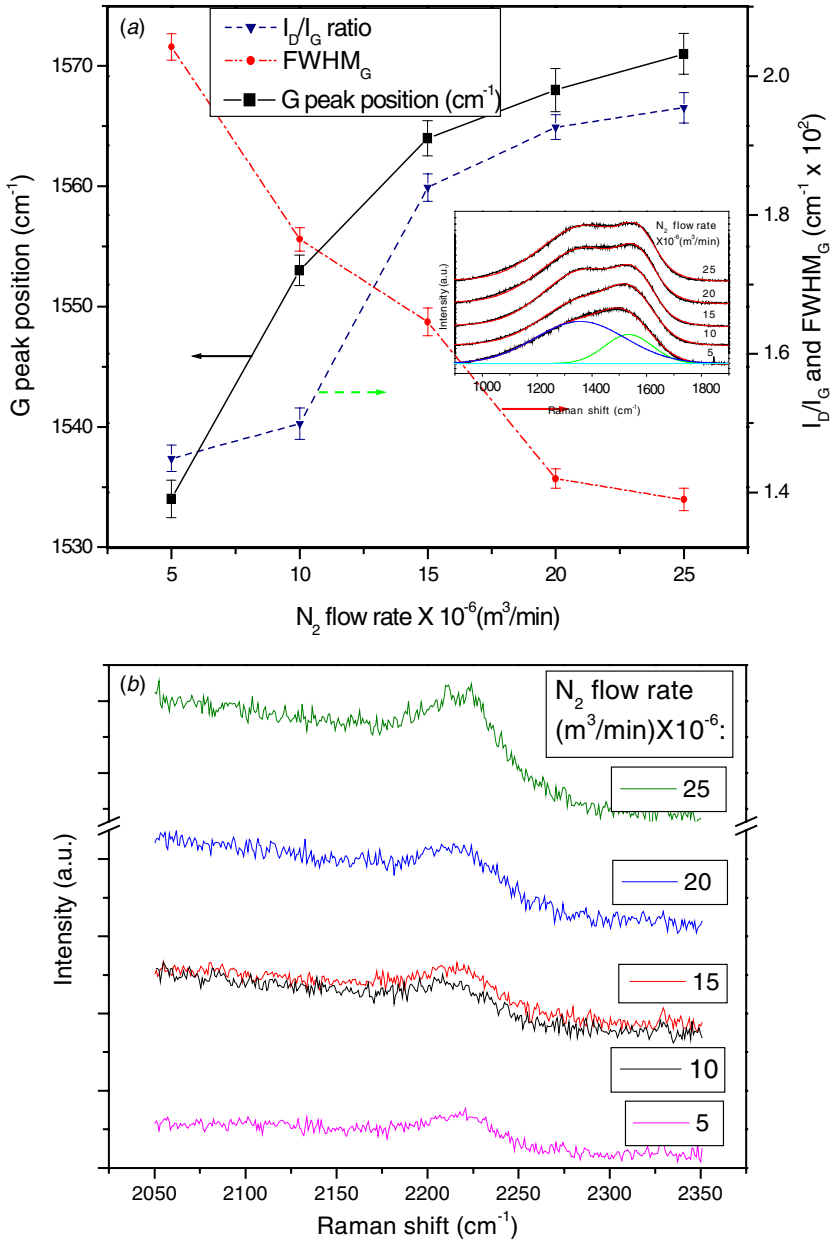

Figure 3. (*a*) Raman G peak position, I_D/I_G ratio and $FWHM_G$ of Si-N-DLC coatings with respect to N_2 flow rate, where the inset shows Raman spectra of the coatings and (*b*) Raman spectra of the coatings for C≡N bonding.

the Si-N-DLC as a solid-lubricant and wear-resistant coating. The friction coefficients of the Si-N-DLC-coated surfaces against the SiC ball are shown in figure 5, where friction coefficients are observed with respect to sliding distance. Despite having the smoothest sample surface, the uncoated Si micro-mold shows a higher coefficient of friction than the Si-N-DLC-coated molds. The coefficients of friction of the samples are in the order of uncoated Si (0.6) > Si-N5-DLC (0.36) > Si-N10-DLC (0.29) > Si-N15-DLC (0.25) > Si-N25-DLC (0.21) > Si-N20-DLC (0.2). The lower friction coefficients with respect to higher N_2 flow rates are attributed to the lubricating effect of the sp^2 bonds in the coatings.

Figure 6 shows the scratch profiles of the Si-N5-DLC- and Si-N25-DLC-coated samples. The critical loads vary with N_2 flow rate under the same scratching conditions. A large number of small chips are observed on the Si-N5-DLC-coated sample (figure 6(*a*)), which indicates that the coating is hard but brittle. Shell-shaped spallation with bigger scratched chips is observed from the Si-N25-DLC-coated sample (figure 6(*b*)). The average critical loads (standard error 1.1–1.2 mN) of the samples are in the order of Si-N5-DLC (375.3 mN) < Si-N10-DLC (388.8 mN) < Si-N15-DLC (397.8 mN) < Si-N25-DLC (405 mN) < Si-N20-DLC (419.5 mN), which also indicates the order of the adhesive strengths of the Si-N-DLC coatings with the Si micro-molds. The different critical loads observed may be mainly caused by residual stresses in the coatings, such as structural mismatch-induced stresses, growth-induced stresses and thermal stresses [27, 28]. Structural mismatch-induced stresses can be neglected for the amorphous DLC coatings. Growth-induced stresses arise from an increase in density that can be related to the sp^3 content in the DLC coatings

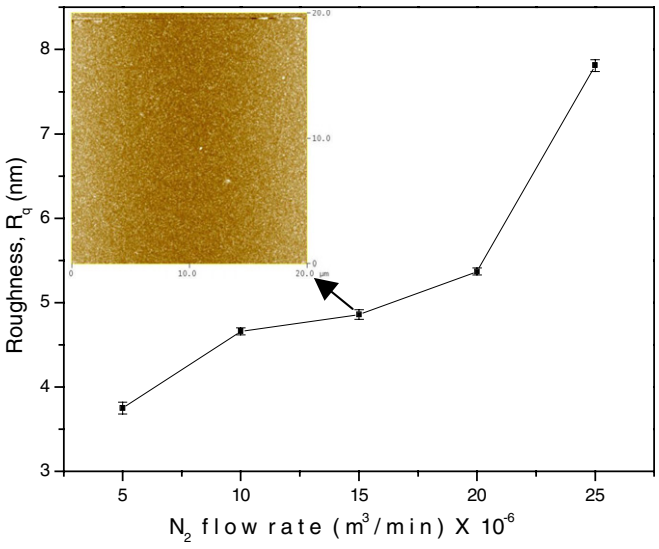

Figure 4. Surface roughnesses of coatings with respect to the N_2 flow rate.

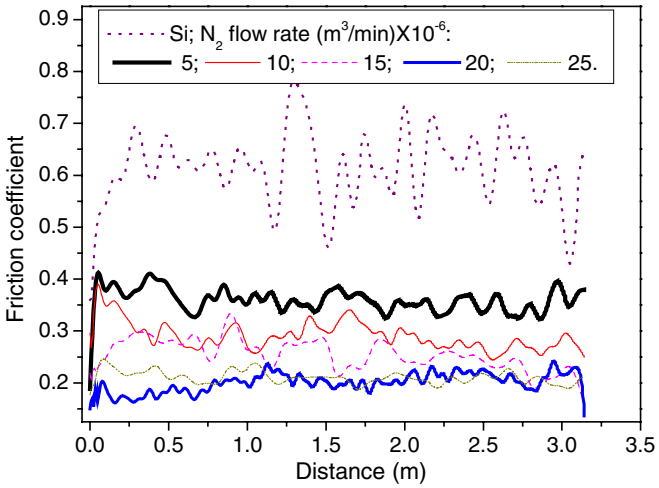

Figure 5. Friction coefficients of uncoated and DLC-coated Si molds versus SiC counter body.

[28, 29]. Thermal stresses are related to different coefficients of thermal expansion between substrate and coating, which are also affected by the bonding structure of the coatings [30]. The Si-DLC:N20-coated sample shows a higher critical load than the Si-N25-DLC one even though the Si-N20-DLC is expected to have a higher sp^3 content, which is attributed to a higher fraction of C≡N sp^1 in the Si-N25-DLC coating.

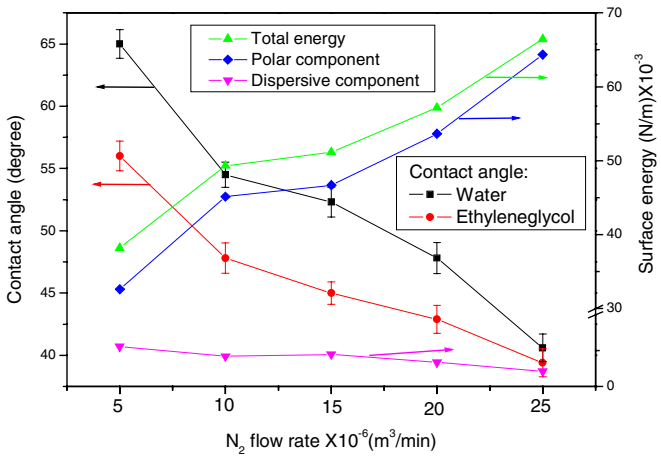

Figure 7. Contact angles of water and ethyleneglycol, total surface energy and its polar and dispersive components with respect to the N_2 flow rate.

The N content in the Si-N-DLC coatings is found to have a great influence on the contact angles of water and ethyleneglycol on the surfaces of the micro-molds. The contact angles measured with respect to the N_2 flow rate are directly connected with the polar and dispersive components of the surface energies calculated as shown in figure 7.

The relationships among surface energy and its dispersive and polar components are expressed as

$$\gamma_{sv} = \gamma_{sv}^{d} + \gamma_{sv}^{p} \quad (1)$$

$$\gamma_{lv} = \gamma_{lv}^{d} + \gamma_{lv}^{p} \quad (2)$$

$$\gamma_{sl} = \gamma_{sl}^{d} + \gamma_{sl}^{p} \quad (3)$$

where γ is the surface energy, the superscripts 'd' and 'p' represent the dispersive and polar components, respectively, and the subscripts 'sv', 'lv' and 'sl' stand for solid–vapor, liquid–vapor and solid–liquid interfaces, respectively.

Young's equation establishes a relationship among surface energies and contact angle (θ) [9, 31]:

$$\gamma_{sv} = \gamma_{sl} + \gamma_{lv}\cos\theta. \quad (4)$$

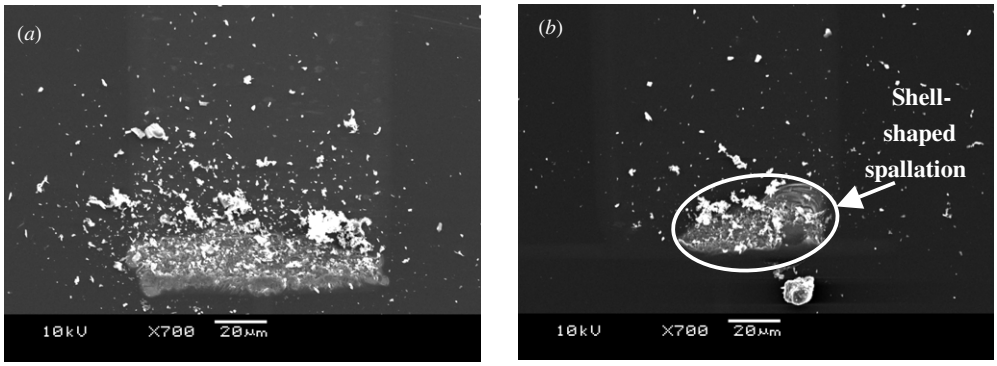

Figure 6. SEM micrographs of the scratched surfaces of (*a*) Si-N5-DLC and (*b*) Si-N25-DLC coatings.

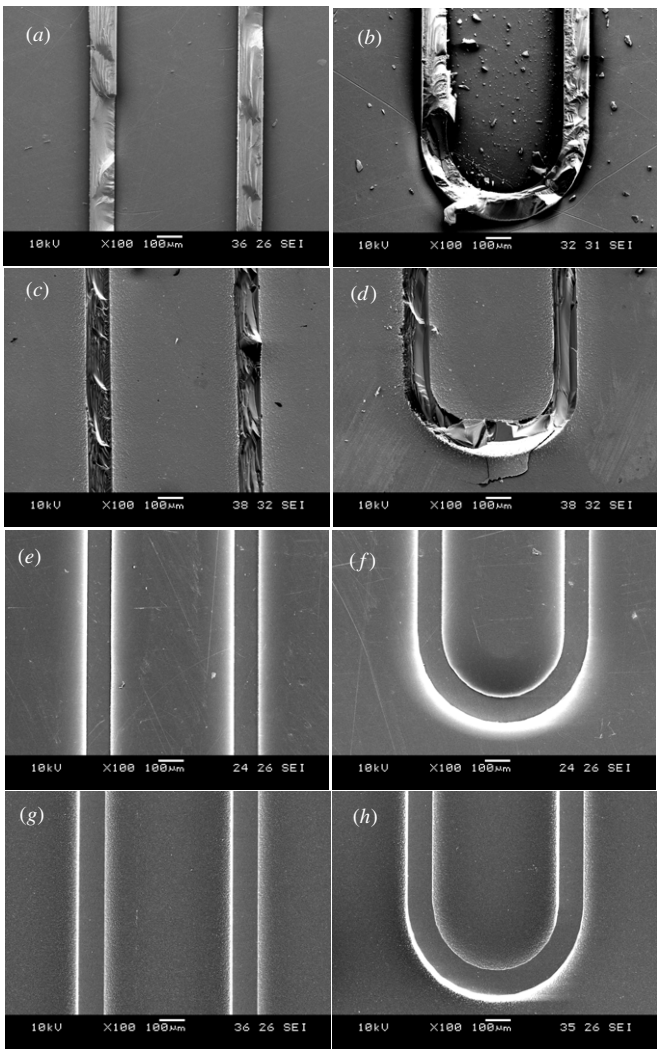

Figure 8. SEM micrographs: (*a*) straight parts and (*b*) round corner of a COC micromolding formed using an uncoated Si micro-mold in the third embossing operation, (*c*) straight parts and (*d*) round corner of microchannels of the same uncoated Si mold after the third embossing operation; (*e*) straight parts and (*f*) round corner of a COC micromolding formed using a Si-N20-DLC-coated Si micro-mold in the eighth embossing operation, (*g*) straight parts and (*h*) round corner of microchannels of the same coated Si mold after the eighth embossing operation.

The dispersive and polar components of surface energies are related by following equations [32]:

$$\gamma_{sl}^{d} = \gamma_{sv}^{d} + \gamma_{lv}^{d} - 2\left(\gamma_{sv}^{d} \cdot \gamma_{lv}^{d}\right)^{1/2} \quad (5)$$

$$\gamma_{sl}^{p} = \gamma_{sv}^{p} + \gamma_{lv}^{p} - 2\left(\gamma_{sv}^{p} \cdot \gamma_{lv}^{p}\right)^{1/2}. \quad (6)$$

From equations (1)–(6), the modified Young's equation is

$$(1 + \cos\theta)\left(\gamma_{lv}^{d} + \gamma_{lv}^{p}\right) = 2\left(\gamma_{sv}^{d} \cdot \gamma_{lv}^{d}\right)^{1/2} + 2\left(\gamma_{sv}^{p} \cdot \gamma_{lv}^{p}\right)^{1/2}. \quad (7)$$

The dispersive and polar components $\left(\gamma_{sv}^{d}\right.$ and $\left.\gamma_{sv}^{p}\right)$ of solid–vapor interface energy are calculated by measuring the water and ethyleneglycol contact angles with their known dispersive and polar component $\left(\gamma_{lv}^{d}\right.$ and $\left.\gamma_{lv}^{p}\right)$ values. From figure 7, the highest surface energy of about 66.5×10^{-3} N m^{-1} is observed from the Si-N25-DLC samples, which is followed by the Si-N20-DLC one (57.2×10^{-3} N m^{-1}). The smallest surface energy (38.2×10^{-3} N m^{-1}) is observed from the Si-N5-DLC-coated mold. A trend is observed in figure 7 that the surface energy of the Si-N-DLC coatings increases with increased N content in the coatings due to increased polar energy component.

A critical step in the hot-embossing process is demolding because the adhesion and friction between the mold and the workpiece can damage the workpiece or distort the micro-features of the workpart. A number of hot-embossing operations were carried out to study the performance of the Si-N-DLC-coated and uncoated Si micro-molds. Thus, the friction force and adhesion between the micro-molds and polymer substrates are the key factors dominating the demolding process, which have to be minimized to obtain a perfect microstructure with high definition. Figures 8(*a*)–(*d*) show the SEM micrographs of different areas of a COC polymer workpiece embossed by an uncoated broken Si micro-mold at the third demolding and the respective areas of the broken mold used. A high surface roughness is created on the sidewall surfaces of the microchannels during deep reactive ion etching (DRIE) fabrication [33], which also promotes a high coefficient of friction and adhesion between the Si molds and the COC moldings. The Si-N-DLC coatings have improved the performance of the Si micro-molds and no broken protrusions and wear debris are observed in figures 8(*e*)–(*h*). The lifetime of the molds is presented in

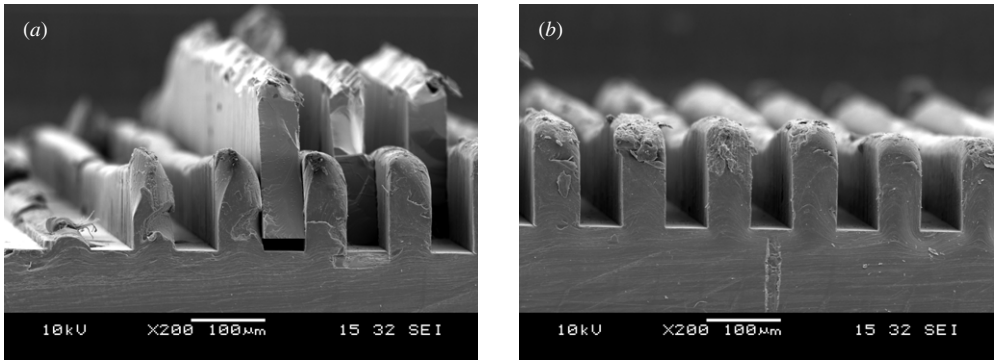

Figure 9. SEM micrographs of (*a*) COC molding formed in the first embossing operation using an uncoated Si micro-mold having parallel channels and (*b*) COC molding formed in the fifth embossing operation using a Si-N20-DLC-coated Si micro-mold having parallel channels.

Table 2. Lifetime of coated and uncoated molds having either zigzag or parallel channels.

Mold type	Uncoated with zigzag channels	Coated with zigzag channels	Uncoated with parallel channels	Coated with parallel channels
Lifetime	2	8	0	5

table 2. From figure 8, it is also observed that the coatings do not delaminate.

A small amount of polymer comes out as a contaminant on the DLC-coated Si molds after a few demolding times, while a little more COC can be found on the uncoated molds. It is also observed that the protrusions from the broken uncoated Si molds stick to the COC polymer with the debris spread over the polymer. The respective uncoated broken Si molds are shown in figures 8(*c*), (*d*), which also indicate improper replications.

The effect of the Si-N-DLC coatings on the replication performance of the micro-molds having a higher aspect ratio and parallel channels is presented in table 2. The replicated COC micromoldings by using the uncoated and DLC-coated Si micro-molds having parallel channels are shown in figure 9. These results indicate that the performance of the Si-N-DLC-coated Si micro-molds is far superior to the uncoated Si micro-molds having both zigzag and parallel microchannels.

4. Conclusions

In this paper, an attempt was made to improve the surface properties of Si micro-molds used in a hot-embossing process, such as friction coefficient, surface energy and critical load. Si-N-DLC coatings were deposited on the Si micro-molds by dc magnetron co-sputtering. Raman analysis of the coatings showed that the G peak position up-shifted with increased N_2 flow rate, indicating increased C–C sp^2 bonds in the coatings. An increased N content in the Si-N-DLC coatings reduced the coefficient of friction of the coated molds, and the Si-N20-DLC-coated mold showed a lowest friction coefficient of about 0.2. The surface energy of the DLC coatings studied by measuring the contact angles of both water and ethyleneglycol increased with higher N content in the coatings. The Si-N25-DLC-coated surface was most hydrophilic and had the highest surface energy of about 66.5×10^{-3} N m^{-1} among the samples used in this study. The Si-N5-DLC-coated mold withstood the lowest critical load of about 375.3 mN, whereas the Si-N20-DLC coated one depicted the highest critical load of about 419.5 mN.

The Si-N-DLC coatings improved the lifetime of both types of Si micro-molds having either zigzag or parallel microchannels, and the coated molds showed a far better replicating performance over the uncoated molds.

References

[1] Ouyang J H, Sasaki S, Murakami T, Zhou Y and Zhang J 2009 Mechanical and unlubricated tribological properties of titanium-containing diamond-like carbon coatings *Wear* **266** 239–47

[2] Sundaram V S 2006 Diamond like carbon film as a protective coating for high strength steel and titanium alloy *Surf. Coat. Technol.* **201** 2707–11

[3] Jones D S, Garvin C P, Dowling D, Donnelly K and Gorman S P 2006 Examination of surface properties and *in vitro* biological performance of amorphous diamond-like carbon-coated polyurethane *J. Biomed. Mater. Res.* B *Appl. Biomater.* **78** 230–6

[4] Milne W I 2003 Electronic devices from diamond-like carbon *Semicond. Sci. Technol.* **18** S81–5

[5] Bonetti L F, Capote G, Santos L V, Corat E J and Trava-Airoldi V J 2006 Adhesion studies of diamond-like carbon films deposited on Ti_6Al_4V substrate with a silicon interlayer *Thin Solid Films* **515** 375–9

[6] Ma T, Hu Y Z, Wang H and Li X 2007 Microstructural and stress properties of ultrathin diamond like carbon films during growth: molecular dynamics simulations *Phys. Rev.* B **75** 035425–8

[7] Oka Y, Kirinuki M, Nishimura Y, Azuma K, Fujiwara E and Yatsuzuka M 2004 Measurement of residual stress in DLC films prepared by plasma-based ion implantation and deposition *Surf. Coat. Technol.* **186** 141–5

[8] Monteiro O R and Ogletree M P D 2003 Investigation of non-hydrogenated DLC: Si prepared by cathodic arc *Surf. Coat. Technol.* **163–164** 144–8

[9] Saha B, Liu E, Tor S B, Khun N W, Hardt D E and Chun J H 2009 Anti-sticking behavior of DLC-coated silicon micro-molds *J. Micromech. Microeng.* **19** 105025

[10] Bendavid A, Martin P J, Comte C, Preston E W, Haq A J, Magdon Ismail F S and Singh R K 2007 The mechanical and biocompatibility properties of DLC-Si films prepared by pulsed DC plasma activated chemical vapor deposition *Diam. Relat. Mater.* **16** 1616–22

[11] Gangopadhyay A K, Willermet P A, Tamor M A and Vassell W C 1997 Amorphous hydrogenated carbon films for tribological applications: I. Development of moisture insensitive films having reduced compressive stress *Tribol. Int.* **30** 9–18

[12] Baba K, Hatada R, Flege S and Ensinger W 2009 Deposition of silicon-containing diamond-like carbon films by plasma-enhanced chemical vapor deposition *Surf. Coat. Technol.* **203** 2747–50

[13] Yeh T A, Lin C L, Sivertsen J M and Judy J H 1993 Friction, wear and elasto-plastic stress analysis of RF-sputtered carbon–nitrogen protective coatings for rigid magnetic storage disks *J. Magn. Magn. Mater.* **120** 314–8

[14] Arora M K, Lettington A H and Waterman D R 1999 Amorphous nitrogen containing carbon films deposited by plasma assisted chemical vapor deposition *Diam. Relat. Mater.* **8** 623–7

[15] Belligundu S, Shiakolas P S, Pandey A and Aswath P B 2008 A systemic approach toward optimization of the hot embossing of poly-L-lactic acid for biomedical applications *J. Biomed. Mater. Res.* B *Appl. Biomater.* **85** 469–77

[16] Fu G, Tor S B, Loh N H and Hardt D E 2009 Micro-hot-embossing of 316L stainless steel micro-structures *Appl. Phys.* A *Mater. Sci. Process.* **97** 925–31

[17] Chien R D 2006 Hot embossing of microfluidic platform *Int. Commun. Heat Mass* **33** 645–53

[18] Song Z, Choi J and You B H 2008 Simulation study on stress and deformation of polymeric patterns during the demolding process in thermal imprint lithography *J. Vac. Sci. Technol.* B **26** 598–605
[19] Guo Y, Liu G, Xiong Y, Wang J, Huang X and Tian Y 2007 Study of hot embossing using nickel and Ni-PTFE LIGA mold inserts *J. Microelectromech. Syst.* **16** 589–97
[20] Komori M, Uchiyama H, Takebe H, Kusuura T, Kobayashi K, Kuwahara H and Tsuchiya T 2008 Micro/nanoimprinting of glass under high temperature using a CVD diamond mold *J. Micromech. Microeng.* **18** 065013
[21] Youn S-W, Noguchi T, Takahashi M and Maeda R 2008 Dynamic mechanical thermal analysis, forming and mold fabrication studies for hot-embossing of a polyimide microfluidic platform *J. Micromech. Microeng.* **18** 045025
[22] Guo Y, Liu G, Zhu X and Tian Y 2007 Analysis of the demolding forces during hot embossing *Microsyst. Technol.* **13** 411–5
[23] Liu F X and Wang Z L 2009 Thickness dependence of the structure of diamond-like carbon films by Raman spectroscopy *Surf. Coat. Technol.* **203** 1829–32
[24] Kaelble D H 1977 A surface energy analysis of bioadhesion *Polymer* **18** 475–82
[25] Liu F X, Yao K L and Liu Z L 2007 Substrate bias effect on structure of tetrahedral amorphous carbon films by Raman spectroscopy *Diam. Relat. Mater.* **16** 1746–51
[26] Ong S-E, Zhang S, Du H and Sun D 2007 Relationship between bonding structure and mechanical properties of amorphous carbon containing silicon *Diam. Relat. Mater.* **16** 1628–35
[27] Wang P, Wang X, Xu T, Liu W and Zhang J 2007 Comparing internal stress in diamond-like carbon films with different structure *Thin Solid Films* **515** 6899–903
[28] Fallon P J, Veerasamy V S, Davis C A, Robertson J, Amaratunga G A J, Milne W I and Koskinen J 1993 Properties of filtered-ion-beam-deposited diamond like carbon as a function of ion energy *Phys. Rev.* B **48** 4777–82
[29] Wang P, Wang X, Xu T, Liu W and Zhang J 2007 Comparing internal stress in diamond-like carbon films with different structure *Thin Solid Films* **515** 6899–903
[30] Marques F C, Lacerda R G, Champi A, Stolojan V, Cox D C and Silva S R P 2003 Thermal expansion coefficient of hydrogenated amorphous carbon *Appl. Phys. Lett.* **83** 3099–101
[31] Chen J S, Lau S P, Sun Z, Chen G Y, Li Y J, Tay B K and Chai J W 2001 Metal-containing amorphous carbon films for hydrophobic application *Thin Solid Films* **398–399** 110–5
[32] Fowkes F M 1963 Additivity of intermolecular forces at interfaces:1. Determination of contribution to surface and interfacial tension of dispersion forces in various liquids *J. Phys. Chem.* **67** 2538–41
[33] Henann D and Anand L 2008 Microscale thermoplastic forming of bulk metallic glasses: numerical simulations and experiments *SMA Int. Conf. and 5th Int. Symp. on Nanomanufacturing* p 40